# Mechanism and Kinetics of Dehydration of Epsomite Crystals Formed in the Presence of Organic Additives

**Encarnación Ruiz-Agudo,† J. Daniel Martín-Ramos,‡ and Carlos Rodriguez-Navarro***

*Departamento de Mineralogía y Petrología, Universidad de Granada, Fuentenueva s/n, 18002 Granada, Spain*

*Received: July 14, 2006; In Final Form: October 10, 2006*

The thermal dehydration of epsomite ($MgSO_4 \cdot 7H_2O$) crystals grown in the presence and absence of organic additives (phosphonates, carboxylic acids, and polyacrylic acid derivatives) was studied by means of thermogravimetry (TG), differential scanning calorimetry (DSC), X-ray thermodiffraction (XRTD), and environmental scanning electron microscopy (ESEM). In situ XRTD analyses (in air, 30% relative humidity) show an epsomite → hexahydrite ($MgSO_4 \cdot 6H_2O$) transition at 25−38 °C, followed by formation of amorphous phase(s) at $T > 43-48$ °C, and $MgSO_4$ crystallization at ∼300 °C. Kinetic parameters ($E_\alpha$ and $A$) were determined for the main dehydration step (25−160 °C), which corresponds to a $MgSO_4 \cdot 7H_2O \rightarrow MgSO_4 \cdot H_2O$ transition, by applying two isoconversional methods to nonisothermal TG data obtained at different heating rates ($\beta = 1$, 3, and 5 $K \cdot min^{-1}$). In situ, hot-stage ESEM observations of the thermal dehydration of epsomite crystals are consistent with the nonisothermal kinetic study and, along with XRTD results, allow us to propose a dehydration mechanism which includes an early nucleation and growth event, followed by the advancement of the reaction interface (3D phase boundary reaction). Both $E_\alpha$ and $A$ values increase in the presence of the most effective crystallization inhibitors tested. H-bonding between additives and epsomite crystal surfaces is consistent with Fourier transform infrared spectroscopy (FTIR) and may account for this effect. The increase of $E_\alpha$ values can be related to the excess energy required to break additive−water bonds in the reactant. These results are likely to further our understanding of the interaction mechanisms between salt hydrates and organic additives which act as growth inhibitors/modifiers.

## 1. Introduction

Many organic molecules display an ability to retard or totally inhibit crystal growth from solution when present at very low (ppm) concentrations.[1] This has made them useful in industrial processes where the growth of crystalline solids must be avoided or controlled. Crystallization inhibitors with extended technological and industrial uses include the following: polyphosphates and phosphonates,[2−9] carboxylic acid derivatives,[10−13] polyelectrolytes,[3,11,14,15] and ferrocyanides.[16,17] Furthermore, growth inhibitors that slow down growth rates of specific faces and thus modify crystal morphology have been used to control crystal bulk shape and particle size distribution, which are critical parameters in many industrial processes.[18] Appropriate control of these parameters usually leads to improved operation or product properties such as density, agglomeration, and redissolution characteristics.[19] However, despite widespread application of crystallization inhibitors/modifiers, their action on nucleation and crystal growth is not yet fully understood.[16] To understand additive−crystal interactions, and to design more effective inhibitor molecules, the molecular-scale mechanisms governing inhibitor−crystal interactions will require more in-depth research.

The manner in which interactions between additives and hydrated salts take place may be further clarified by using thermal analysis to study dehydration reactions of salt hydrates formed in the presence and absence of organic additives. In general, dehydration reactions proceed stepwise through a series of intermediate reactions involving the decomposition of one phase and the formation of a new one.[20] The kinetic parameters of these reactions have a physical meaning and can be used to help disclose solid reaction mechanisms. Kinetic calculations may offer interesting conclusions regarding such mechanisms, although in some cases such calculations may not be the most efficient method for their determination,[21] and additional micrometer-scale observation might be required.[22]

Although interactions between sparingly soluble salts and organic additives have been the subject of numerous investigations,[23] little is known about the effects of organic additives on the crystallization of highly soluble salts, such as magnesium sulfate. Epsomite ($MgSO_4 \cdot 7H_2O$) is widely used in medicine (acute management of cardiac arrhythmia and asthma),[24] in agriculture as a source of Mg (fertilizer), in Kraft pulp bleaching process, amino acid production, ore processing, textile manufacture and finishing, detergent formulation, manufacture of high-fructose products, and rubber processing.[25] It is a raw material for manufacturing various chemicals containing Mg and is also applied in the field of dosimetric measurement.[26] Additives may thus be critical for controlling epsomite crystals shape, size, and reactivity and may offer an opportunity to control undesired salt caking.[16]

Several studies have been published on the thermal decomposition of salt hydrates,[28−32] including epsomite.[33−39] Epsomite readily transforms into hexahydrite ($MgSO_4 \cdot 6H_2O$) due to loss of extra-polyhedral water (i.e., water that is not in octahedral coordination with Mg). This transition is reversible and occurs at a temperature of 298 K at 50−55% relative humidity (RH),

* Corresponding author. Phone: +34 958 246616. Fax: +34 958 243368. E-mail: carlosrn@ugr.es.
† E-mail: encaruiz@ugr.es.
‡ E-mail: jdmartin@ugr.es.

10.1021/jp064460b CCC: $37.00 
Published on Web 12/15/2006

and at lower temperatures when water activity diminishes.[40] Detrimental caking typically occurs during such phase transition. Epsomite−hexahydrite transition is facilitated by the structural similitude between these two phases: both consist of $SO_4$ tetrahedra and $Mg(O,H_2O)_6$ octahedra.[27] Upon further $T$ increase, phases with $5H_2O$ (pentahydrite), $4H_2O$ (starkeyite), $3H_2O$, $2H_2O$ (sanderite), $1.5H_2O$, $1H_2O$ (kieserite), and $0.5H_2O$ moles are formed.[33−39] Most of them are crystalline, although formation of amorphous phases has been reported.[27,33] At $T$ higher than ~300 °C, crystalline anhydrous $MgSO_4$ forms.[33] Despite the numerous works dedicated to the study of epsomite thermal dehydration, the mechanisms of such stepwise complex process are still poorly understood.

Recently, the study of epsomite dehydration mechanism and kinetics has regained interest because of their implications in the Martian water cycle,[27] in the formation of Martian outflow channels,[41] and in the identification of possible hydrated salts in Europa satellite.[40,42] To our knowledge, however, no publications yet exist which focus on the dehydration of salt hydrates formed in the presence of organic additives. The aim of this paper is to study the thermal dehydration of pure and additive-doped epsomite crystals in order to disclose how the interaction between organic additives and hydrated salt crystal surfaces occurs and to gain some insights into the mechanism of such dehydration process. A second aim of this research is to evaluate the potential of the combined use of in situ X-ray thermodiffraction (XRTD), in situ environmental scanning electron microscopy (ESEM), and thermogravimetry (TG) kinetic analyses to study the mechanisms of solid-state dehydration reactions.

## 2. Experimental Section

**Materials.** A special laboratory setup was designed[16] to allow for crystallization of salt solution following free evaporation in a controlled environmental chamber ($T = 25 \pm 2$ °C; RH = $40 \pm 10\%$). Epsomite crystals were obtained in batch crystallization tests carried out using this setup. Magnesium sulfate saturated solution was prepared using anhydrous solid (Sigma-Aldrich, reagent plus) and deionized water. Nondissolved crystals were removed by decanting the saturated solution. Prior to evaporation of the magnesium sulfate solution, organic additives were dosed at concentrations of $10^{-4}$, $10^{-3}$, $10^{-2}$, and $10^{-1}$ M. The additives used were as follows: (1) poly(carboxylic) acids and derivatives (citric acid, CA; aspartic acid sodium salt, AAS; poly(acrylic acid, sodium salt), PA) and (2) poly(phosphonic) acids such as HEDP (1-hydroxyethylidene-1,1-diphosphonic acid), ATMP (aminotri(methylene phosphonic acid)), and DTPMP (diethylenetriaminepentakis(methylphosphonic acid)). All additives were purum (Fluka). The pH was raised to 8 using NaOH (Panreac, purissimum) since it then promotes maximum interaction between salt crystals and the deprotonated functional groups of the additives.[23]

Crystals formed in magnesium sulfate solution with 0.1 M additive concentration were collected and stored in a closed cabinet at 20 °C and 75% RH (to avoid epsomite dehydration). A 0.1 M additive concentration was selected because it promotes the greatest inhibitory capability. Crystallization inhibition, defined here as the percentage of growth inhibition (GI), was measured as the percent increment in critical supersaturation (i.e., supersaturation reached at the onset of crystallization) of Mg sulfate solution with and without additives.[23] Powdered samples for analysis were obtained by gentle grinding of the single crystals in an agate mortar (final crystal size, 0.5−1 mm). Such samples were subjected to TG and differential scanning calorimetry (DSC) analyses, as well as to X-ray diffractometry and Fourier transform infrared spectroscopy (FTIR; Nicolet IR200) using the KBr pellet method. Raw TG data were used to model the kinetics of the dehydration process.

**Powder X-ray Thermodiffraction**. In situ XRTD data were collected on a Philips PW-1710 diffractometer, using Cu Kα radiation ($\lambda = 1.5406$ Å) and equipped with a home-built heating device. The heating system includes a Pt temperature probe, a precision $T$ controller, and a thyristor power regulator firing a halogen lamp (75 W, 220 V) that provides up to 200 °C to the sample. A detailed description of the heating device can be found elsewhere.[43,44] A water cooling system was used to prevent overheating. Diffraction patterns were collected in air (30% RH) from 4.5 min scans (10−35° $2\theta$ explored area) at 1 °C intervals (i.e., heating rate of 0.22 K·min$^{-1}$), upon warming from 20 to 198 °C. Such a low heating rate was selected because higher heating rates (up to 1 K·min$^{-1}$; achieved by increasing the goniometer scan rate and increasing $T$ intervals) did not affected the temperature of the phase transition but yielded less well-defined diffraction peaks. Additional diffraction data of samples heated in air at 300 °C (300 min) using an electric oven were recorded to identify possible crystallization of anhydrous magnesium sulfate. Diffraction analyses were also performed on samples heated and rehydrated for 24 h in a closed cabinet at 20 °C and 75% RH to elucidate if the dehydration reaction was reversible.

**ESEM Observations**. Dehydration of epsomite single crystals was observed in situ, at high magnification, using an environmental scanning electron microscope equipped with a heating stage (hot stage). ESEM images were obtained on a FEI Quanta 400 ESEM operated at an accelerating voltage of 20 kV. The microscope was fitted with a FEI water-cooled 1000 °C specimen heating stage with a high-temperature controller and a K-type thermocouple for temperature monitoring. A high-temperature gaseous secondary electron detector with a pressure-limiting aperture, mounted directly above the specimen on the heating stage, was used for electron imaging. During heating, the detector−sample distance was set to ~10 mm and the ESEM chamber pressure was set at 2.5 Torr water vapor. Such water vapor pressure is equivalent to that of ambient air at 20 °C and 15% RH. Crystals of epsomite with size in the same range of that used in TG/DSC and XRTD analyses were glued onto $Al_2O_3$ cups with a thin layer of conductive carbon cement. This was done to ensure that the crystals were well-attached to the cup surface and to maintain reasonable heat conductance. No sample precoating with carbon or gold was required for ESEM observations. This is one of the main advantages of ESEM since it avoids artifacts when observing phase transitions in situ.[45] The sample was heated from 17 to 450 °C at an average heating rate of 15 °C/min. A constant temperature was maintained during image acquisition, which was done after an equilibration time of 15 min. Note that even though it is strongly recommended that microscopical observation should be performed to properly evaluate thermal dehydration reactions,[31] to our knowledge only two studies have taken advantage of the ESEM for performing in situ high-magnification analyses of such reactions.[44,46]

**Thermal Analysis (TG and DSC).** Dehydration of epsomite crystals was initially studied in flowing (100 cm$^3$·min$^{-1}$) air atmosphere using a Shimadzu TGA-50H thermogravimetric analyzer equipped with a Mettler-Toledo AX26 Delta Range microbalance and a Shimadzu DSC-50Q differential scanning calorimeter. Temperature was raised from 25 to 500 °C at a heating rate of 5 K·min$^{-1}$. In each measurement about 40 mg of specimen was weighed into a platinum crucible, and weight

loss data were collected at regular time intervals. An online Nicolet 550 FTIR spectrometer was used to perform infrared analyses of the gases evolved during thermal dehydration of epsomite and/or thermal decomposition (oxidation) of adsorbed organic additives. To perform kinetic analysis of the dehydration process, additional multi-heating-rate TG tests ($\beta = 1$, 3, and 5 K·min$^{-1}$) were carried out in flowing (100 cm$^3$·min$^{-1}$) nitrogen. Flowing nitrogen was used to ensure that no oxidation of the organic additives occurred during epsomite thermal decomposition. To minimize mass effect, about 5 mg of specimen was used for kinetic analyses.

**Kinetic Analysis: Theory and Calculations.** Since decomposition of a solid occurs as a heterogeneous reaction, a kinetic analysis of this reaction should take into account several phenomena, such as the chemical reaction, mass and heat transfer, and physical changes in the solid. Most of the methods developed to describe the kinetics of thermal decomposition of solids introduce two simplifying assumptions: (i) the temperature at any point in the solid is the same as it is in the external fluid at any given moment, and (ii) the controlling step in the reaction rate does not change throughout the transformation.[47]

In our case, the overall reaction studied, which reportedly involves several intermediate steps,[33,39] is

$$MgSO_4 \cdot 7H_2O(s) \xrightarrow{\Delta T} MgSO_4 \cdot nH_2O(s) + (7-n)H_2O(g)$$

The dehydrated fraction, α, is calculated using

$$\alpha = \frac{m_i - m_t}{m_i - m_f} \tag{1}$$

where $m_i$ and $m_f$ are the initial and final masses in milligrams, respectively, and $m_t$ is the mass at the specific time $t$. An adequate kinetic description in terms of the reaction model and of the Arrhenius parameters of a thermally stimulated reaction can be obtained using a single-step kinetic equation:[48]

$$\frac{d\alpha}{dt} = k_d(T)\, f(\alpha) \tag{2}$$

where $k_d(T)$ is the apparent specific rate constant of the decomposition reaction, α is the fraction of epsomite decomposed at time $t$, and $f(\alpha)$ is the reaction model. The reaction model $f(\alpha)$ usually represents an empirical function. Mathematical expressions for several functional forms of $f(\alpha)$ are listed elsewhere.[49]

The temperature dependence of the rate constant is obtained from the Arrhenius equation. Considering a linear heating rate of $dT/dt = \beta$, eq 2 becomes[48,50]

$$\frac{d\alpha}{f(\alpha)} = \frac{A}{\beta}\exp\left(\frac{-E}{RT}\right)dT \tag{3}$$

where $A$ is the preexponential factor and $E$ is the activation energy.

Different approaches have been proposed to solve eq 3. Model-fitting and model-free kinetic approaches have been widely applied to nonisothermal and isothermal dehydration processes. Model-fitting methods solve eq 3 by force-fitting experimental data to different $f(\alpha)$ model functions. Kinetic parameters can be evaluated once a $f(\alpha)$ mechanism has been selected. Model-fitting methods give excellent fits for both isothermal and nonisothermal data but yield highly uncertain values of the Arrhenius parameters when applied to nonisothermal data.[51] In fact, experimental data obtained at a single heating rate can be force-fitted by several $f(\alpha)$ models, yielding Arrhenius parameters that vary by an order of magnitude.[48] Moreover, model-fitting methods yield a constant value of the activation energy for the overall process, without taking into account the multiple-step nature of solid-state processes.[49,52] On the other hand, isoconversional methods provide a model-free approach that gives reliable kinetic information from nonisothermal data.[53] The model-free approach has been applied here to nonisothermal dehydration of epsomite crystals. The basic assumption of the isoconversional methods is that the reaction model is not dependent on heating rate.[53] In the present work, the kinetic analysis of TG data was carried out using two multi-heating-rate methods: the Flynn, Wall, and Ozawa (FWO) integral isoconversional method and the nonlinear isoconversional method proposed by Vyazovkin (VYA).[54] These methods yield the activation energy $E_\alpha$ at each given conversion α, which is independent of the reaction model. For isoconversional computations 100 equidistant values of conversion were chosen. The $T_\alpha$ values related to these conversions were found by nonlinear interpolation. The fraction dehydrated (α) was calculated from experimental TG data. Values of ($d\alpha/dT$) were calculated for a set of ~100 values of α for each heating rate and smoothed with the method of moving an average of 25 terms.

The FWO method involves measuring the temperatures corresponding to fixed values of α from experiments performed at different heating rates, $\beta$, and plotting $\ln(\beta)$ against $1/T_\alpha$

$$\ln(\beta) = \ln\left[A\frac{f(\alpha)}{d\alpha/dT}\right] - \frac{E_\alpha}{R\,T_\alpha} \tag{4}$$

the slopes of such plots give $-E_\alpha/R$.

According to the VYA method, for a set of $n$ experiments carried out at different heating rates, the activation energy can be determined at any particular value of α by finding the value of $E_\alpha$ for which the function[51]

$$\sum_{i=1}^{n}\sum_{j\neq 1}^{n}\frac{I(E_\alpha,T_{\alpha,i})\beta_j}{I(E_\alpha,T_{\alpha,j})\beta_i} \tag{5}$$

is a minimum, where the temperature integral in eq 5 is

$$I(E_\alpha,T_\alpha) = \int_0^{T_\alpha}\exp\left(\frac{-E}{RT}\right)dT \tag{6}$$

The values of $I(E_\alpha,T_\alpha)$ may be found by numerical integration or with the help of approximations. In our case, we have used the Senum-Yang approximation with $x = -E/RT$,

$$I(E_\alpha,T_\alpha) \approx p(x) = \exp(-x)/x(x^2 + 10x + 18)/(x^3 + 12x^2 + 36x + 24) \tag{7}$$

The minimization procedure is repeated for each α value to find the dependence of the activation energy on the extent of conversion.[54]

We used the method proposed by Vyazovkin and Lesnikovich[55] to estimate the preexponential factor $A$ in both FWO and VYA models. This method relies on the apparent compensation dependence

$$\ln A = aE + b \tag{8}$$

This relation yields $A$ values once $E$ values are determined. For a simple process, $A$ and $E$ will be constant over the entire range of transformation, whereas for a complex one there will be a

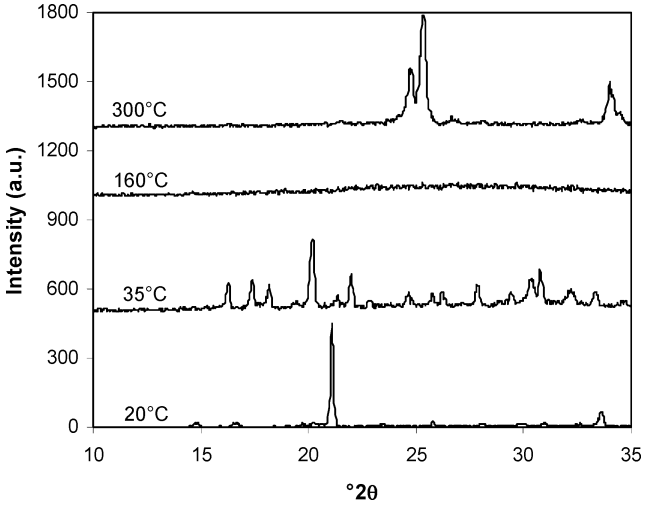


**Figure 1.** Selected X-ray diffraction patterns of epsomite crystals submitted to heating (in air, 30% RH). Phases present: epsomite (20 °C), hexahydrite (35 °C), amorphous hydrate (160 °C), and anhydrous $MgSO_4$ (300 °C).

dependence on α. Considering such dependence, Arrhenius parameters were computed from

$$\ln\left[\left(\frac{d\alpha}{dT}\right)\beta f(\alpha)^{-1}\right] = \ln A_\alpha - \frac{E_\alpha}{RT_\alpha} \quad (9)$$

which is the linearized form of eq 3 for the different $f(\alpha)$-models listed by Vyazovkin.[49] ln $A_\alpha$ and $E_\alpha$ pairs were thus used to determine the parameters $a$ and $b$ in eq 8.[56]

### 3. Results and Discussion

**Features of Epsomite Thermal Dehydration in Air**. Figure 1 shows selected XRTD patterns of phases formed upon heating epsomite crystals in air (30% RH) up to 300 °C. Only three crystalline phases were observed: epsomite (20−38 °C), hexahydrite (24−48 °C), and anhydrous $MgSO_4$ ($T \sim 300$ °C). At 43 °C < $T$ < 300 °C an amorphous phase was detected. Neither Mg−DTPMP nor Mg−PA salts were detected in the case of additive-doped epsomite crystals. Figure 2 shows a detail of the epsomite−hexahydrite−amorphous (hydrate) transition. Our XRTD results are consistent with those reported by Heide.[33] This author observed epsomite−hexahydrite transition at 46 °C and the formation of an amorphous phase following destruction of hexahydrite at 93 °C. Heide observed no other crystalline phase until dehydrated $MgSO_4$ crystallized at 273 °C. Note that epsomite−hexahydrite transition $T$ is strongly affected by water vapor partial pressure.[37,40] Unfortunately, most published results on epsomite−hexahydrite transition $T$ do not provide information regarding the RH (or $P_{H_2O}$) at which experiments were performed. The latter may explain the scattering in reported epsomite−hexahydrite transition temperatures.[35,36,56] Figure 2 shows that epsomite−hexahydrite and hexahydrite−amorphous transitions occur at slightly higher $T$ in the presence of additives. This is most noticeable in the case of DTPMP-doped crystals (Figure 2b). X-ray diffraction analyses of rehydrated $MgSO_4$ as well as rehydrated amorphous phase(s) formed at $T$ < 198 °C show formation of epsomite. This confirms that the dehydration reaction is fully reversible.

TG and DSC curves for pure epsomite crystals are shown in Figure 3a. Quantitative data calculated from TG and DSC measurements are shown in Tables 1 and 2, respectively. No stable intermediates could be clearly identified, most probably

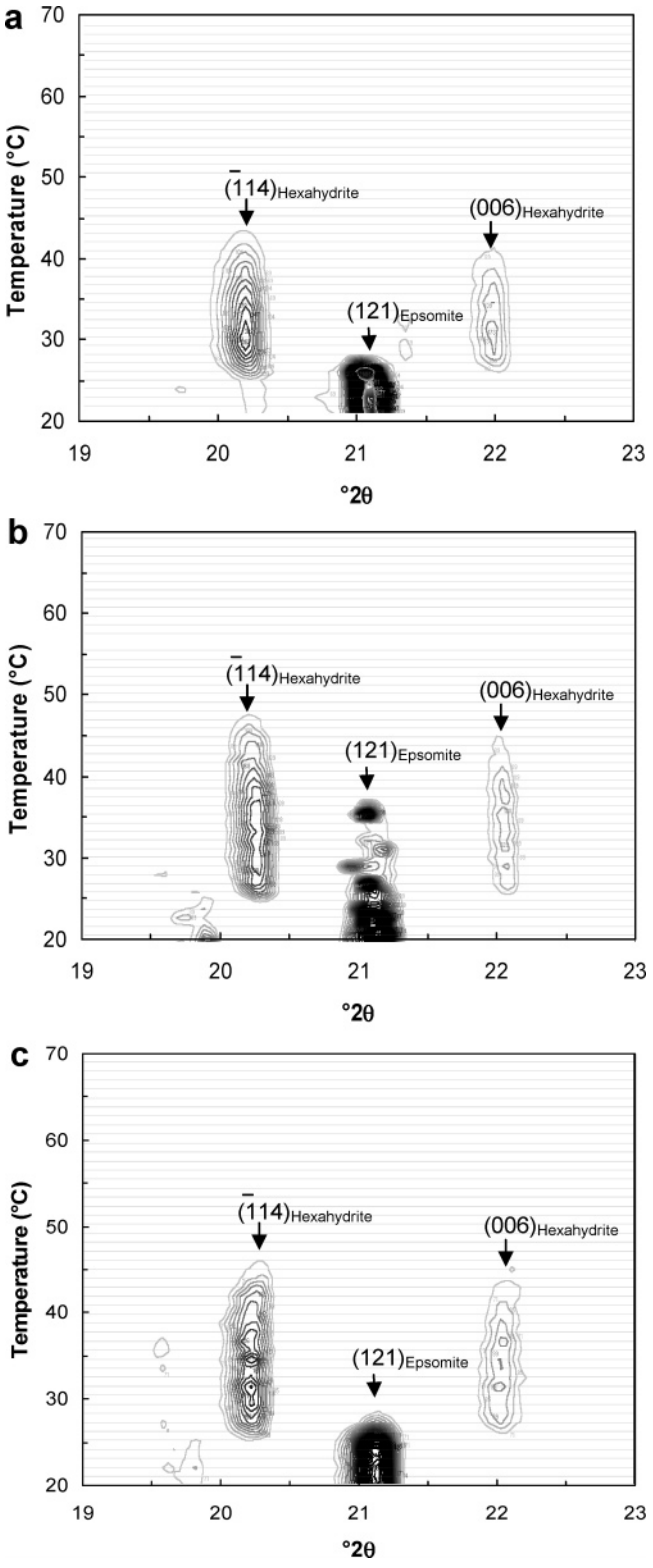


**Figure 2.** Two-dimensional ($2\theta$ (deg) vs $T$) representations of XRTD peak intensities (contour lines) of the following: (a) pure epsomite, (b) DTPMP-doped epsomite, and (c) PA-doped epsomite submitted to heating. It is shown that the intensity of the main epsomite diffraction peak diminishes while hexahydrite main peaks appear, and their intensity diminishes as an amorphous phase forms at higher $T$ (i.e., when peak intensity is reduced to background levels).

due to mass effects and the high heating rates used. Dehydration took place in two main steps (I and II). These two steps were easily identifiable in DSC records (Figure 3a). Step I, which was the most significant, expanded from ∼25 to ∼200 °C. DSC

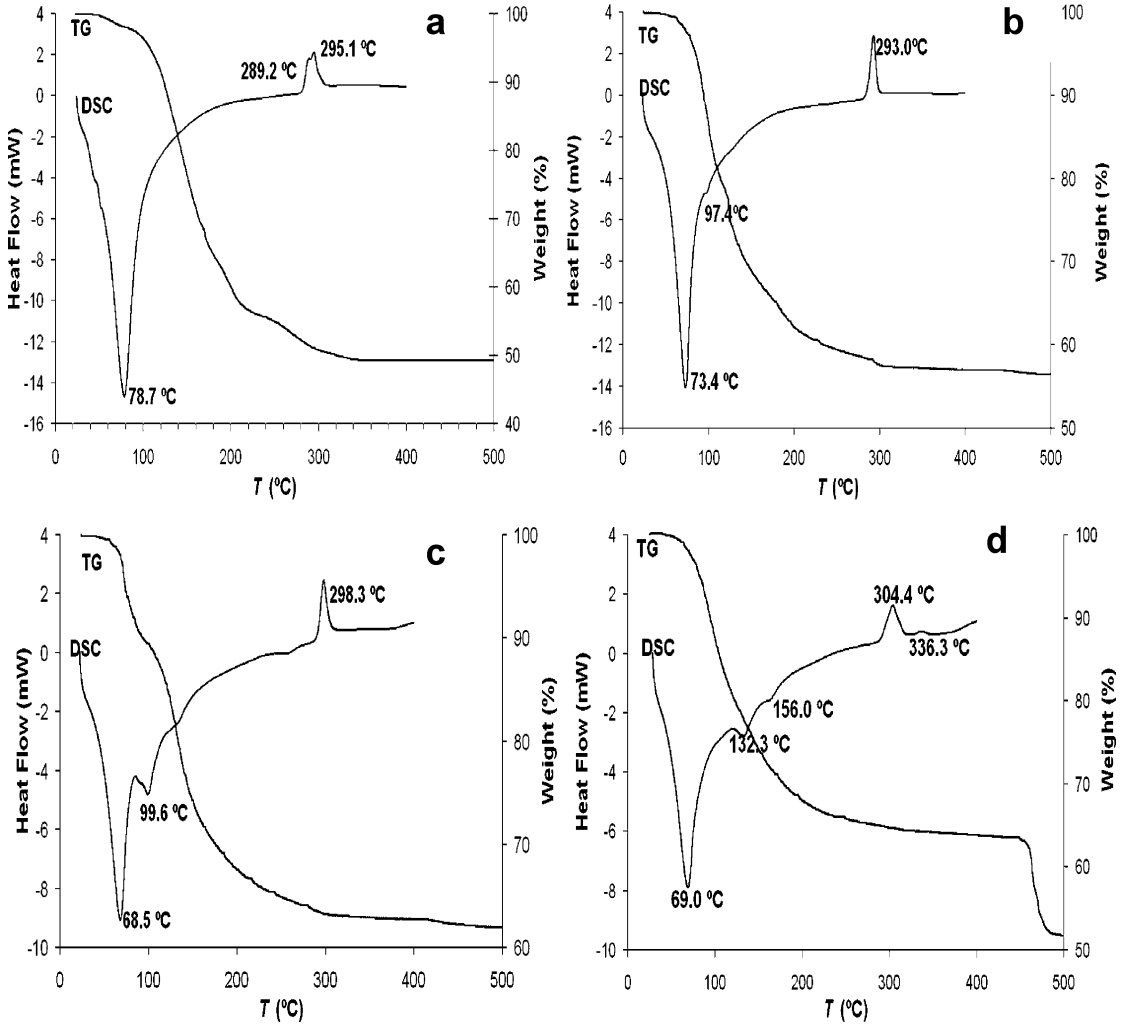


**Figure 3.** TG and DSC plots of magnesium sulfate heptahydrate crystals formed in the absence and in the presence (0.1 M and pH 8) of additives ($\beta$ = 5 K·min$^{-1}$; 25−500 °C $T$ range; flowing air atmosphere): (a) control, b) ATMP-doped epsomite, (c) DTPMP-doped epsomite, and (d) PA-doped epsomite.

**TABLE 1: Parameters Obtained from TG Measurements ($\beta$ = 5 K min$^{-1}$) of Epsomite Crystals Dehydration**

| | | TG measurements | |
|---|---|---|---|
| sample | dehydration step | $T_{onset}$, °C | mass loss, % |
| control | 1st | 25.3 | 41.7 |
| | 2nd | 141.6 | 8.0 |
| DTPMP doped | 1st | 22.7 | 40.0 |
| | 2nd | 157.2 | 7.1 |
| PA doped | 1st | 22.3 | 35.6 |
| | 2nd | 156.1 | 9.7 |

showed a broad endothermic peak with a minimum at 68.5−78.7 °C that belongs to the dehydration of epsomite ($MgSO_4$·$7H_2O$) to kieserite ($MgSO_4$·$H_2O$). In a second step (∼200−325 °C), dehydration due to loss of the last water molecule led to $MgSO_4$.[53] This final transition included an exothermic reaction associated with the recrystallization of an amorphous precursor,[33] as confirmed by XRTD results showing the formation of crystalline anhydrous $MgSO_4$ at $T \sim 300$ °C (Figure 1). The final weight loss was 51.4 ± 1.9%, a value which is close to the theoretical 51.22% corresponding to the loss of 7 water moles. Step I corresponded to a weight loss of 42.7 ± 1.5%, which corresponds to the loss of $6H_2O$ moles. Crystals formed in the presence of ATMP, DTPMP, and PA showed additional peaks in the DSC record that belong to intermediate dehydration steps (Figure 3). PA is a thermally stable polymer, degrading in inert atmosphere (nitrogen) at $T$ > 380 °C (heating rate of 10 K·min$^{-1}$).[57] The TG curve steep slope in the $T$ range of 460−480 °C (Figure 3d) corresponded to PA decomposition. No significant changes were observed in the DSC or TG curves of crystals formed in the presence of HEDP, CA, and AAS (data not shown). The latter compounds were not effective in promoting epsomite crystallization inhibition; therefore, no further analyses were performed using epsomite crystals grown in their presence. FTIR analyses of evolved gases (Figure 4) showed water absorption bands at 3857, 3744, 3620, 1700, and 1514 cm$^{-1}$ as well as $CO_2$ absorption bands at 3729, 3632, 2366, 2330, and 676 cm$^{-1}$. $CO_2$ emission occurred following thermal decomposition of crystals formed in the presence of ATMP, DTPMP, and PA (Figure 4). In the case of PA-doped epsomite, the FTIR spectrum was much more complex than that of the other additives. Absorption bands of $C_2H_6$ (3137, 3014, 1426, and 951 cm$^{-1}$), $CH_4$ (3019 and 1303 cm$^{-1}$), and CO (2182 and 2115 cm$^{-1}$) were also detected (Figure 4d). These results confirm the presence of additives in epsomite crystals when they display inhibitory capability as in the cases of ATMP and DTPMP that reach GI values of 88 and 204%, respectively,[58] as well as PA, which reaches a GI value of 128%. FTIR analyses of epsomite crystals formed in the presence of phosphonates show the existence of hydrogen bonds between additive functional groups and water molecules in $MgSO_4$·$7H_2O$, an observation which suggests that they are incorporated into the epsomite structure.[58] Similar results were obtained in the case

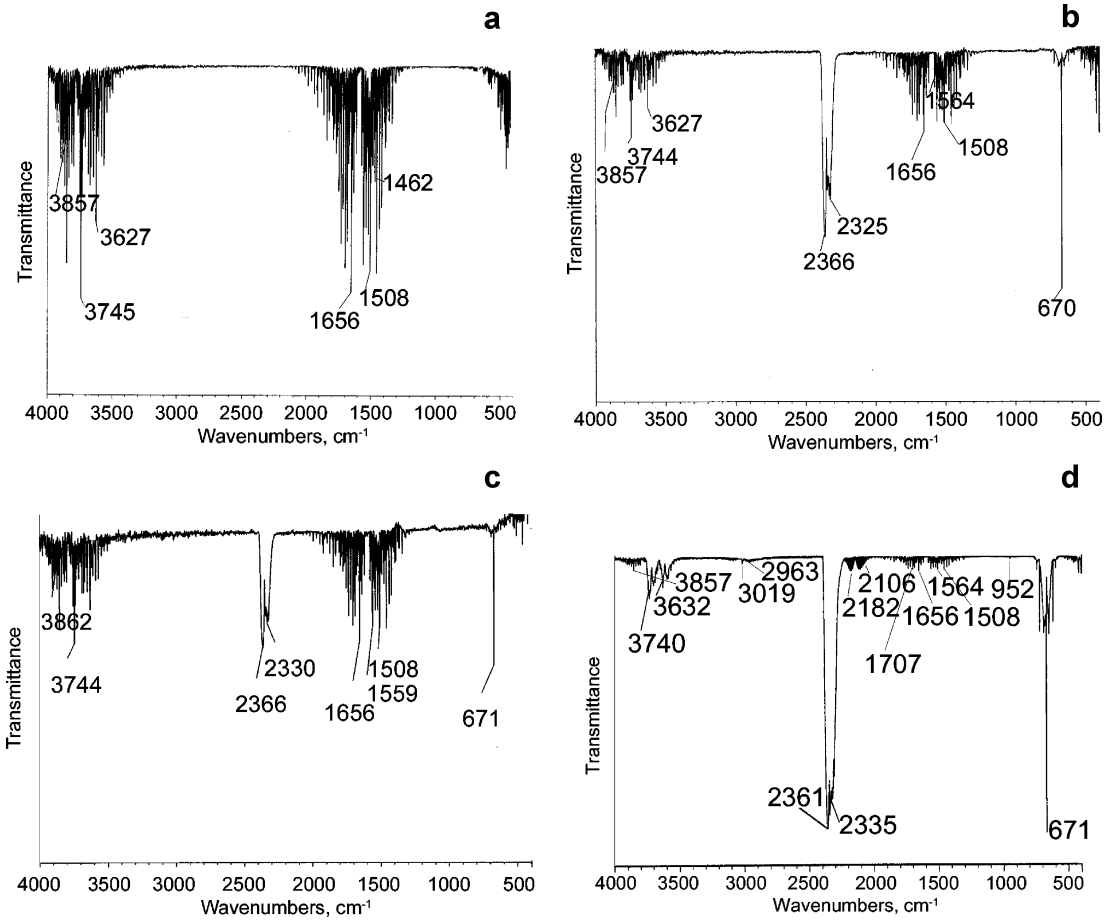


**Figure 4.** Integrated FTIR spectra of evolved gases for pure and additive-doped epsomite crystals ($\beta = 5$ K·min$^{-1}$; 25−500 °C $T$ range; flowing air): (a) control, (b) ATMP-doped epsomite, (c) DTPMP-doped epsomite, and (d) PA-doped epsomite.

**TABLE 2: Parameters Obtained from DSC Measurements ($\beta = 5$ K min$^{-1}$) of Epsomite Crystals Dehydration**

| | | DSC measurements | | | |
|---|---|---|---|---|---|
| sample | peak | $T_{onset}$, °C | $T_{endset}$, °C | $T_{peak}$, °C | $\Delta H$, kJ mol$^{-1}$ |
| control | 1st endo | 50.0 | 102.2 | 78.7 | −266 |
| | 1st exo | 282.5 | 302.6 | 295.1 | 13 |
| DTPMP doped | 1st endo | 41.3 | 84.1 | 68.5 | −200 |
| | 2nd endo | 111.1 | 86.0 | 99.6 | −9 |
| | 1st exo | 291.3 | 305.6 | 298.3 | 9 |
| PA doped | 1st endo | 43.4 | 85.5 | 69.0 | −148 |
| | 2nd endo | 120.7 | 146.6 | 132.3 | −5 |
| | 1st exo | 290.1 | 317.6 | 304.4 | 8 |

of PA-doped epsomite crystals (Figure 5). H-bonding between PA functional groups and epsomite water molecules resulted in a significant broadening of the hydroxyl absorption band.[59] Mass balance calculations yield a concentration of 5.5 ± 2.9 wt % DTPMP and 14.8 ± 3.5 wt % PA, incorporated into epsomite crystals.

**Kinetic and Morphological Analyses.** Kinetic analyses of TG data were performed for pure and PA-, DTPMP-doped epsomite crystals (i.e., the additives showing the highest inhibitory capability). As mentioned above, PA is a thermally stable polymer,[57] while DTPMP thermal decomposition takes place in inert atmosphere (helium) at around 240 °C ($\beta = 20$ K·min$^{-1}$).[60] It is therefore expected that additive thermal decomposition will not overlap with the first step of epsomite dehydration. Figure 6 shows raw TG data for epsomite crystals first dehydration step in flowing $N_2$ ($\beta = 1$ K·min$^{-1}$). To facilitate comparison, additive-doped weight loss data in Figure 6 were adjusted following subtraction of the additive mass. The use of a lower amount of sample (ca. 5 mg) and lower heating rates (1−5 K·min$^{-1}$) helped disclose the presence of metastable intermediate phases, not clearly observed when higher amounts of sample and higher heating rates were used. Furthermore, it was observed that the first dehydration stage was completed at $T \sim 130-160$ °C. Within this first dehydration stage, the following intermediates were observed in the control: $MgSO_4$·$6H_2O$, $MgSO_4$·$5H_2O$, $MgSO_4$·$4H_2O$, $MgSO_4$·$3H_2O$, $MgSO_4$·$2H_2O$, $MgSO_4$·$1.5H_2O$, and $MgSO_4$·$H_2O$. Such intermediates have been observed previously.[33,37,39] $MgSO_4$·$6H_2O$, $MgSO_4$·$2H_2O$, $MgSO_4$·$1.5H_2O$, and $MgSO_4$·$H_2O$ intermediates were also observed in additive-doped samples. Other intermediates were observed in the latter samples but were poorly defined or corresponded to unknown phases. On the other hand, Figure 6 shows that the dehydration of each intermediate phase occurs at higher $T$ in additive-doped crystals. These results show that the dehydration rate is strongly affected (reduced) by the additives.

Figure 7 shows α vs $T_\alpha$ plots for pure epsomite crystal dehydration obtained at heating rates of 1, 3, and 5 K·min$^{-1}$.

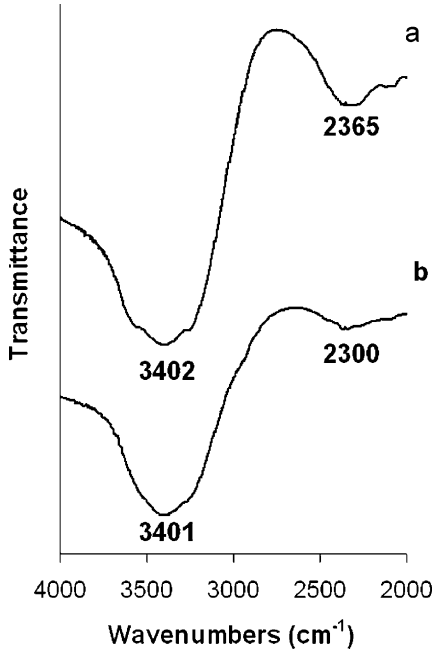


**Figure 5.** Hydroxyl absorption bands in the FTIR spectrum of the following: (a) pure and (b) PA-doped epsomite crystals. The most significant change occurs in the hydroxyl band at ~2300 $cm^{-1}$.

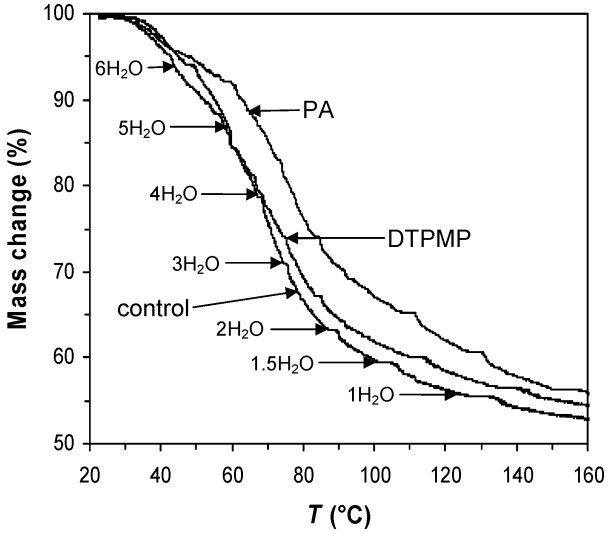


**Figure 6.** TG plots showing multistep dehydration of pure (control) and DTPMP- and PA-doped epsomite ($\beta = 1$ K·$min^{-1}$; flowing nitrogen atmosphere). Only the main dehydration stage is shown.

**TABLE 3: Parameters *a* and *b* Used in Equation 8 for the Calculation of ln *A***

| | $\beta = 1$ K·$min^{-1}$ | $\beta = 3$ K·$min^{-1}$ | $\beta = 5$ K·$min^{-1}$ |
|---|---|---|---|
| $a \times 10^4$ (mol·$J^{-1}$) | 3.4 | 3.2 | 3.1 |
| $b$ | −0.3865 | −0.3445 | −0.3275 |
| $r^2$ | 0.9919 | 0.9928 | 0.9926 |

Calculations by isoconversional methods revealed a dependence of the activation energy on the transformation degree, which is an indication of the complex character of this process.[59] Figure 8 shows the transformation-degree dependence of $E_\alpha$ and $A_\alpha$ values calculated using both FWO and VYA methods. $A_\alpha$ values were calculated using the *a* and *b* parameters shown in Table 3. Note that there is a convergence of $E_\alpha$ and $A_\alpha$ values obtained by both isoconversional methods at $\alpha < 0.5$. Nonetheless, a slight divergence is found at higher $\alpha$ values. The results obtained using the FWO method are more scattered that those

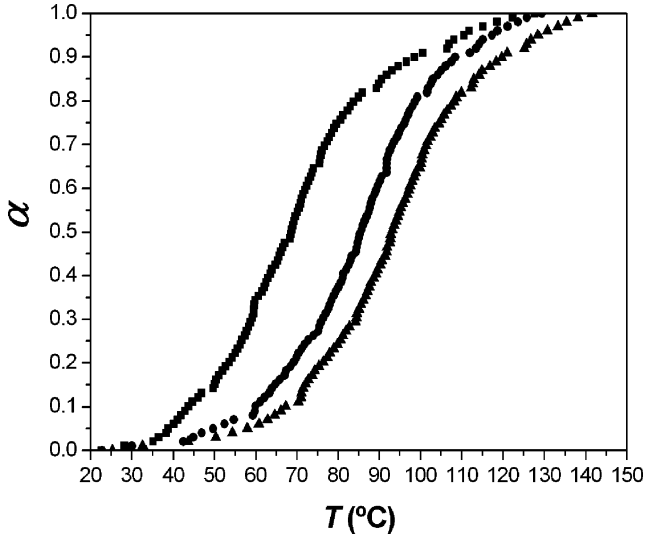


**Figure 7.** Experimental α-temperature (*T*) curves for the dehydration of epsomite in flowing nitrogen, obtained at different heating rates (■, 1 K·$min^{-1}$; ●, 3 K·$min^{-1}$; ▲, 5 K·$min^{-1}$).

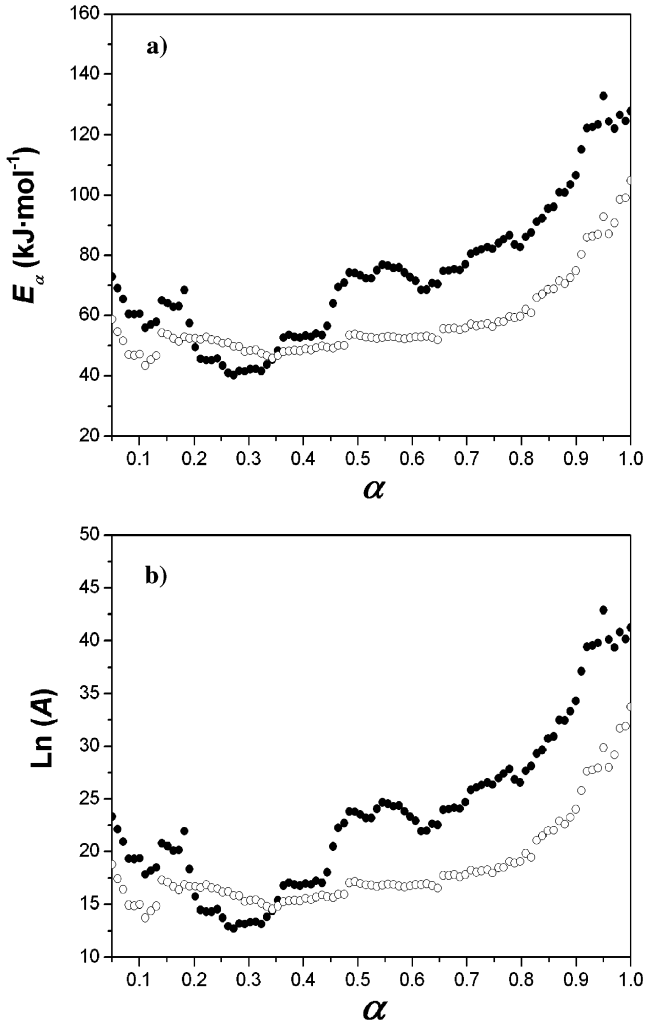


**Figure 8.** Dependence of (a) activation energy, $E_\alpha$, and (b) preexponential factor, *A*, on the extent of conversion α, determined by FWO (●) and VYA (○) methods for the nonisothermal dehydration of epsomite crystals.

obtained using the VYA method. Therefore we selected the latter method to compare kinetic values of additive-doped crystals (see below). $E_\alpha$ values range between ~40 and ~140 kJ/mol.

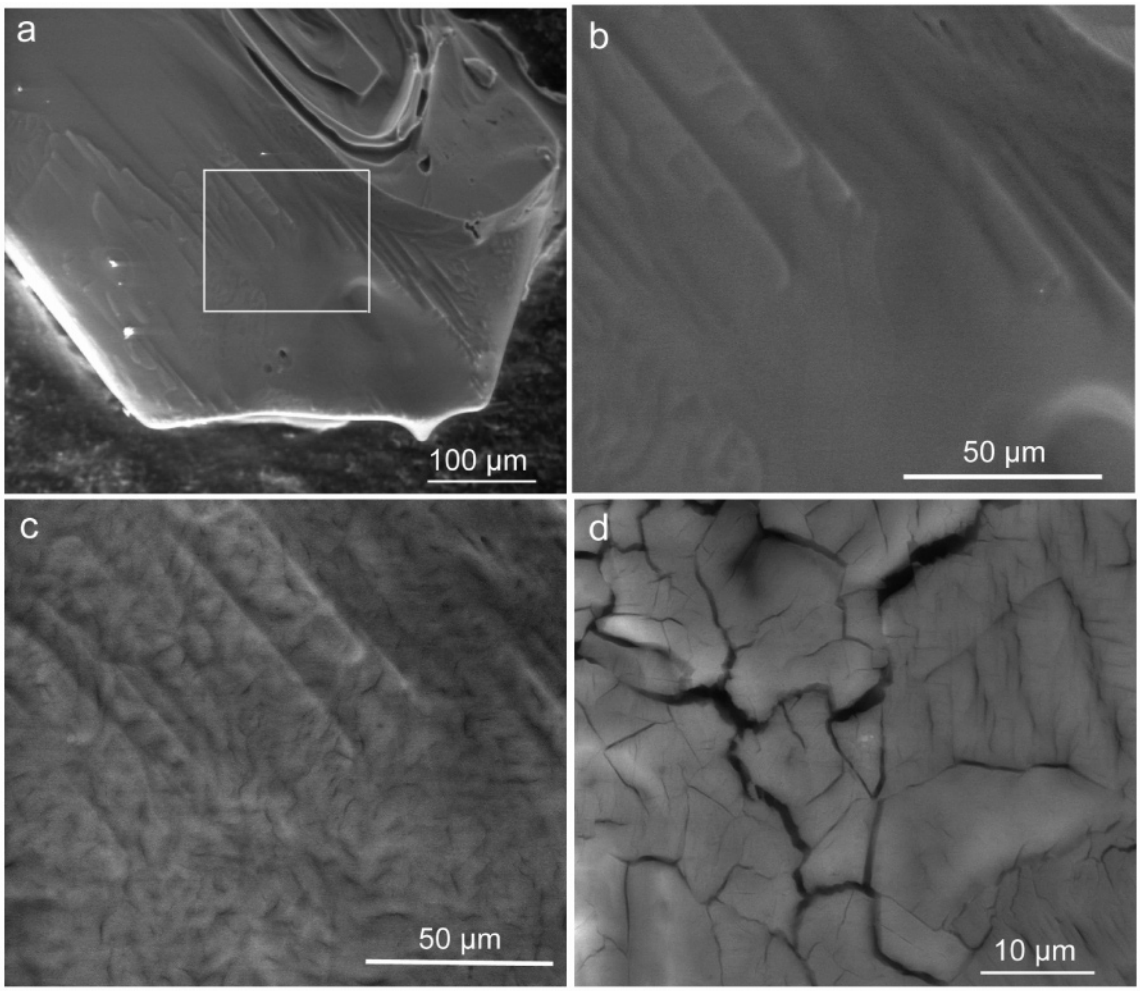


**Figure 9.** ESEM photomicrographs of an epsomite crystal before (a and b) and after (c and d) thermal dehydration: (a) low magnification of a prismatic epsomite crystal showing the {110} form; (b) detail of squared area in a before dehydration (at 17 °C); (c) same area as in b after dehydration at 30 °C; (d) detail of cracks in the crystals shown in a.

The initial $E_\alpha$ value of 60 kJ/mol (at $\alpha = 0.05$) is in good agreement with published values for epsomite−hexahydrite nonisothermal decomposition.[33] At $\alpha = 0.12$ the minimum $E_\alpha$ value of 40 kJ/mol is reached. Such a value is close to that of water evaporation.[31] At $0.15 < \alpha < 0.8$ a nearly constant value of ca. 50 kJ/mol is observed. The latter suggests that once the dehydration reaction starts (i.e., nucleation event), it easily proceeds due to destruction of the reactant structure and subsequent water evaporation. In the final stage of dehydration a value of 100−140 kJ/mol is reached. This latter value is in good agreement with reported $E_\alpha$ values for $MgSO_4{\cdot}3H_2O$−$MgSO_4{\cdot}H_2O$ conversion.[39] The $E_\alpha$ vs $\alpha$ curve has a concave shape, which is typical of reversible dehydration reactions.[61] This is consistent with X-ray diffraction results.

Vyazovkin has indicated that, in general, thermally stimulated reactions do not follow a single kinetic law.[49] As a consequence, the formulation of a mechanistic model based on purely kinetic results is rather difficult. The detailed kinetic interpretation of epsomite complex dehydration process, which involves a number of intermediate stages[33−39] and, possibly, different reaction mechanisms, therefore requires additional information. It is very useful to examine the reaction morphology and/or geometry by microscopy, to establish the physicogeometric features of the reaction.[62] Figures 9, 10, 12, and 13 show ESEM dehydration sequences (from 17 to 450 °C; 2.5 Torr water vapor) of epsomite single crystals grown in the absence and presence of organic additives. Although the dehydration behavior is slightly different in powdered and single-crystal materials, the information from the latter is crucial to elucidate the kinetics of the former.[63] Nonetheless, it should be pointed out that the crystal size of powdered samples used in TG/DTA as well as XRTD analyses is very similar to that of crystals used in the ESEM experiments. Parts a and b of Figure 9 show representative detailed microscopic views of an epsomite crystal surface at 17 °C. They show that the starting material had relatively smooth surfaces. Figure 9c shows a detail of the epsomite surface depicted in Figure 9b once (partial) dehydration had occurred at 30 °C. Numerous micrometer-sized pits and cracks were observed. In other areas of the same crystal, larger cracks also developed (Figure 9d). Crack formation and propagation occurred quickly when the dehydration conditions were imposed ($T \sim 25-30$ °C). At 30 °C the crystal surface was already covered with cracks, and no further crack formation or propagation occurred when $T$ was raised (Figure 10). The reduction of the crystal volume with increasing $T$ is shown in Figure 10b. Such volume reduction contributed to the narrowing of cracks. No melting was observed over the full range of tested $T$, an observation which confirms the solid-state nature of epsomite dehydration. Galwey[31] has indicated that errors in the kinetic (and mechanistic) analysis of thermally activated reactions are commonly associated with the erroneous assumption that dehydration occurred without melting, which is not the case in a number of dehydration reactions. As suggested by this author, our microscopic observations have been critical to disclose the

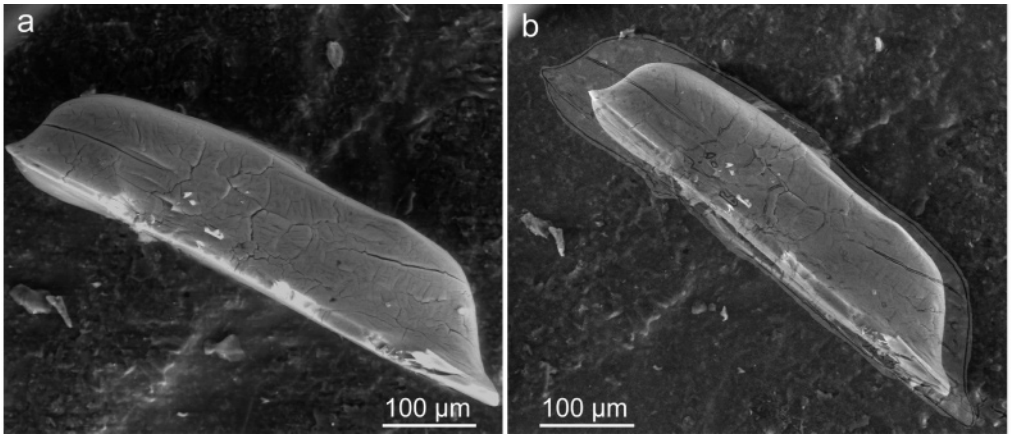


**Figure 10.** Contraction of epsomite crystal during thermal dehydration: (a) cracks formed at 30 °C; (b) same crystal at 450 °C. The contour of the crystal shown in a is overlapped for comparison.

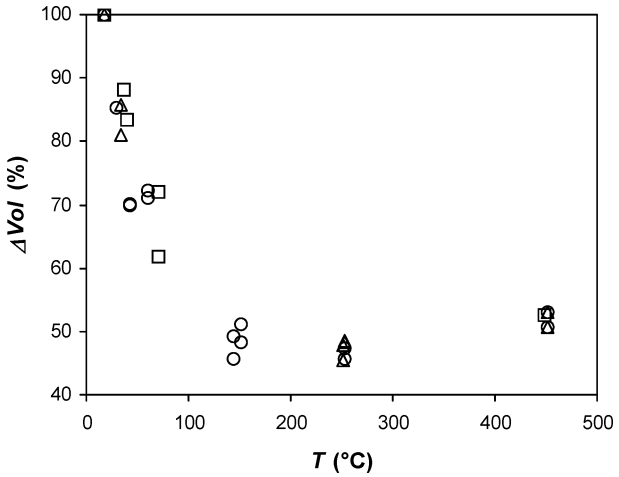


**Figure 11.** Volume change (Δvol) vs *T* of pure (○), PA-doped (△), and DTPMP-doped (□) epsomite crystals dehydrated in the ESEM chamber at 2.5 Torr water vapor.

absence of melting. Figure 11 shows the evolution of epsomite crystal volume vs *T* calculated from ESEM photomicrographs. It is worth pointing out that crystal length reduction was nearly isotropic (i.e., similar in the [100], [010], and [001] directions), even though $MgSO_4{\cdot}nH_2O$ phases are not cubic. This suggests that there is no clear crystallographic control in the advancement of the reaction. A similar feature has been reported for the thermal dehydration of alum, which is not cubic either.[31] Interestingly, the volume vs *T* curve was parabolic with decreasing absolute value of the slope up to 250 °C, when full dehydration occurred. At higher *T*, the slope became positive. The shape of the curve for $T < 250$ °C is consistent with a falling rate dehydration process (i.e., deceleratory process). For $T > 250$ °C, a slight volume increase took place most probably due to thermal expansion of the anhydrous phase. Note that there is not a direct correspondence (in terms of *T* of phase transition) between ESEM observations and TG/DSC results due to the lower water vapor pressure in the ESEM chamber (2.5 Torr), if compared with the laboratory (5.3 Torr, at 20 °C and 30% RH). Thus, dehydration reactions systematically took place at lower *T* within the ESEM chamber. However, as we will discuss bellow, there is a clear mechanistic correspondence between the ESEM observations and the results of the kinetic analysis.

Overall, ESEM observations are typical for a 3D interface advancement-controlled deceleratory reaction.[31] Such reaction can be classified as WET3 following Galwey's scheme.[31] The nucleation step is rapidly achieved, because the formation of a product that retains much of the reactant structure requires little reorganization. This is consistent with Heide's observations on the formation of hexahydrite after nonisothermal dehydration of epsomite which fitted an Avrami-Erofeev nucleation and growth reaction model.[33] Because the dehydrated product is pseudomorphic with the original reactant, the initial surface nucleation sites cannot be distinguished. Once a superficial layer of product is formed, further reaction is mainly limited to the reaction interface. Gradually, the reaction interface moves toward the interior of the crystal. This mechanism is entirely consistent with the nonisothermal kinetic study, showing an initial increase in the values of the kinetic parameters followed by their slight reduction at intermediate $\alpha$ values (nucleation and growth stage) and a final increase at higher $\alpha$ values (diffusion-controlled interface advancement).

ESEM observations, XRTD results, and kinetic behavior can be explained considering two different stages in the overall epsomite to kieserite dehydration process. During the first stage, nuclei of the new phase (i.e., hexahydrite) rapidly form and grow. As a consequence, the reaction interface enlarges, and the reaction rate increases (*reaction rate increasing period*).[31] Following further growth of crystal nuclei, the reaction interface reaches a maximum, as does the apparent reaction rate. Cracking close to the reaction zone occurs as shown by the ESEM analysis, most probably due to the fact that strain associated with water removal is greater than that which can be sustained by the product structure.[31] Cracks provide channels for water escape. These two processes, i.e., nuclei growth and crack formation, take place almost simultaneously and are associated with the first decrease in the values of $E_\alpha$ an $A_\alpha$ at $\alpha = 0.1$ (Figure 8a). Such a degree of decomposition corresponds to the loss of $0.58H_2O$ moles (i.e., ongoing conversion between epsomite and hexahydrite). Note that epsomite surfaces were covered with cracks at an early stage of the decomposition process, and no further cracks developed at higher *T* (ESEM observations). Limited diffusion is required for the displacement of water from the water-vacated site to the cracks. This is a probable reason for the increase in $E_\alpha$ values at $0.1 < \alpha < 0.15$. A conversion of 0.17 corresponds to the loss of $1H_2O$ mole (i.e., full conversion of epsomite into hexahydrite). Note that such initial conversion involves the loss of extra-polyhedral water (i.e., loosely bonded).[27] Afterward, water loss is less easy, and this explains why $E_\alpha$ and $A_\alpha$ reach a maximum at $\alpha \sim 0.15$ when dehydration of hexahydrite starts.

A reduction in the kinetic values occurs at $0.15 < \alpha < 0.35$. This has been associated with the transition from higher hydrates

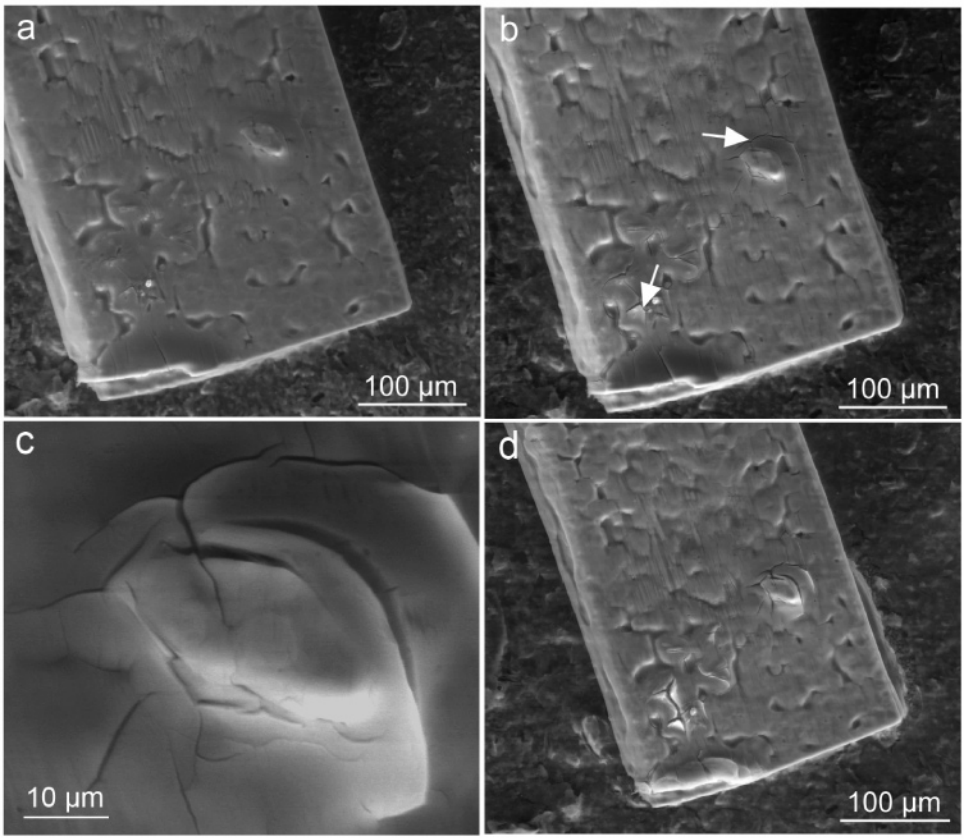


**Figure 12.** ESEM images of PA-doped epsomite crystal dehydration: (a) at 17 °C, before dehydration; (b) at 150 °C (note the formation of a few cracks (arrows)); (c) detail of the cracked area pointed by the upper arrow in b; (d) at 450 °C (note the volume reduction).

(i.e., hexahydrite) to lower hydrates. Actually, a value of $\alpha = 0.33$, corresponds to the loss of $2H_2O$ moles. During this second stage a continuous layer of solid product forms and increases the resistance to water diffusion, without a new generation of cracks. As a consequence, at high conversion degrees ($\alpha > 0.7$) the reaction changes from its surface kinetic period to its diffusion period. The reactant−product interface moves toward the interior of the particles. The increase in diffusion resistance experienced by water molecules passing through the product layer will have a direct impact in the reaction kinetics. The obstruction in water vapor removal caused by the product surface layer and the subsequent reduction in the overall reaction rate are called "impedance" and "arrest", respectively.[32]

Dehydration results in an overall increase in close packing and density, due to higher influence of covalent and/or ionic bonding in the product. This is consistent with the observed volume reduction and limited crack sealing (ESEM results). Therefore, water vapor escape will be more difficult in the densely packed structure of the lower hydrates, where the remaining water molecules are more strongly linked to the nonvolatile crystal constituents than to each other.[63] These latter factors will contribute to the overall increase in the kinetic parameters at $\alpha > 0.70$ (Figure 8).

ESEM observations of the dehydration of additive-doped epsomite crystals show that shrinking with increasing $T$ followed the same trend as in the case of pure epsomite crystals (Figure 11). Figure 11 shows that the rate of volume reduction was slightly lower in additive-doped epsomite crystals than in pure epsomite during the early stages of dehydration ($T < 70$ °C). The reduction in the shrinkage rate was highest in the case of DTPMP-doped espsomite crystals (i.e., the additive displaying the highest crystallization inhibition capability). Figures 12 and 13 show ESEM images of the dehydration of additive-doped epsomite crystals. Note that DTPMP causes a significant habit change in epsomite crystals: from equilibrium-shaped bulky {110} forms (Figure 9a) to acicular or prismatic-shaped crystals (Figure 13). The latter suggests that DPTMP acts also as a growth modifier. Figures 12 and 13 show that a lower density of cracks developed in additive-doped epsomite crystals if compared with pure epsomite crystals (Figure 10). Channels were apparently less important for water removal in additive-doped epsomite. In fact, the reaction appeared to be mainly controlled by water diffusion. This may explain why the initial period of acceleration ($\alpha < 0.15$) was not that important in additive-doped epsomite crystal dehydration (Figure 14). This also explains previously discussed changes in shrinkage rate in additive-doped crystals. When additives were present, $E_\alpha$ was higher than in pure epsomite at low conversion values, i.e., during the epsomite−hexahydrite phase transition (Figure 14). Such $E_\alpha$ increase was particularly evident in the case of PA-doped crystals. On the other hand, $E_\alpha$ increased substantially at high conversion values in the case of PA-doped crystals (Figure 14). In the latter case, two relative $E_\alpha$ maxima were observed at $\alpha \sim 0.67$ and $\alpha \sim 0.75$, corresponding to $MgSO_4 \cdot 2H_2O$ and $MgSO_4 \cdot 1.5H_2O$ metastable phases, respectively.

During the dehydration process water must be released from the hydrate, requiring the rupture of hydrogen bonds and, possibly, coordination links as well as any other interactions that contribute to hydrate stability. The magnitude of $E_\alpha$ can be related to the rupture of these links in the reactant.[31] Thus, variations (increases) in activation energy in the early stages of dehydration could be linked to variations in water binding forces within the hydrate. The reduction in the dehydration rate of epsomite crystals formed in the presence of additives was shown

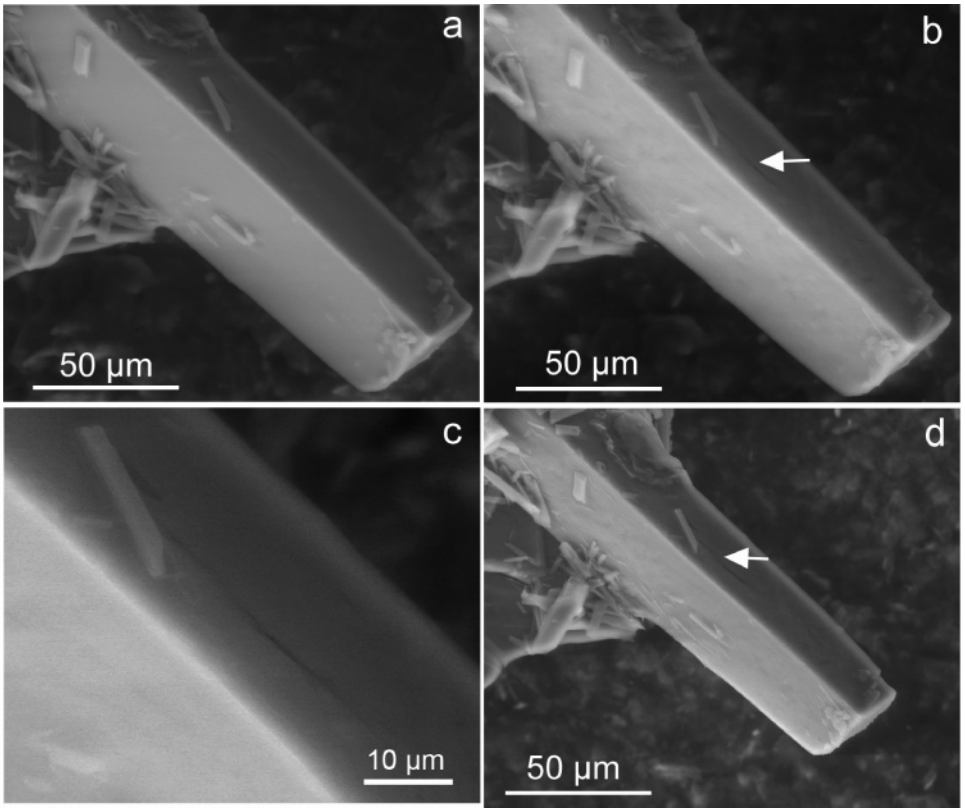


**Figure 13.** ESEM images of DTPMP-doped epsomite crystal dehydration: (a) at 17 °C, before dehydration (note the prismatic shape, showing overdevelopment along the *c*-axis); (b) at 150 °C (note the formation of only a few cracks (arrow)); (c) detail of crack pointed by the arrow in b; (d) at 450 °C (note the volume reduction).

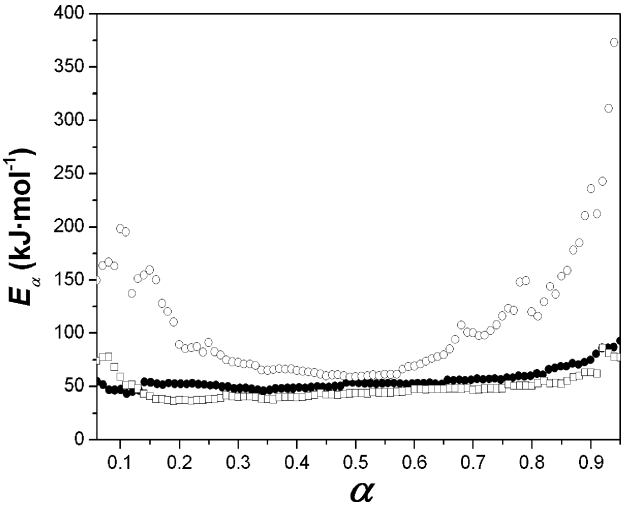


**Figure 14.** Dependence of the activation energy, $E_\alpha$, on the extent of conversion, α, determined by VYA method for the nonisothermal dehydration of epsomite crystals: (●) pure, (○) PA-doped, and (□) DTPMP-doped.

by XRTD (Figure 2) and TG results (Figure 6). Such reduction is consistent with the establishment of H-bonds between hydration water in the crystal and functional groups in the additives, causing the observed reduction in the ease of dehydration. On the other hand, it is suggested that the high amount of PA (a large polymer with molecular weight of 2100) on PA-doped crystals could create an impervious layer for water vapor escape once dehydrating samples start contracting (i.e., it may help to seal cracks). Such effect may contribute to the very high $E_\alpha$ values reached in PA-doped samples at $\alpha > 0.5$ (Figure 14).

## 4. Conclusions

The powerful combination of analytical tools and kinetic analyses yields mechanistic insights into the modes of water loss in pure and additive-doped epsomite crystals. Pure epsomite displays two main stages in the thermal dehydration process: stage I, which involves the stepwise loss of $6H_2O$ moles, and stage II, which involves the loss of $1H_2O$ mole. While a stepwise loss of water is also observed in the case of epsomite crystals formed in the presence of additives, their dehydration rate is reduced. Application of isoconversional methods to raw TG data enables the kinetic parameters ($E_\alpha$ and $A_\alpha$) to be calculated for the first (main) dehydration step (25−160 °C). These kinetic calculations, along with in situ, high-magnification, hot-stage ESEM observations and in situ XRTD analysis of epsomite crystal thermal dehydration, allow us to propose a mechanistic model for this dehydration process. The kinetic and morphological studies show that the first dehydration step of epsomite crystal is complex and can be described as a deceleratory reaction controlled by interface advancement. During the latest stages of the reaction a reduction in the reaction rate is observed. This is associated with the obstruction of the diffusional removal of the gaseous product by the surface product layer and the stronger bonding of $H_2O$ molecules in lower hydrates. Overall this reaction can be classified as a type WET 3: interface reaction, three dimensions, according to Galwey.[31]

The kinetic parameters $E_\alpha$ and $A_\alpha$ are substantially increased in the presence of additives. These results are consistent with the establishment of hydrogen bonds between the tested organic molecules and structural water in epsomite and the lower hydrates resulting from the progress of the dehydration reaction. These results support the presence of additives (DTPMP and PA) in the epsomite crystal lattice. However, the prevalence of H-bonding suggests that a structural matching between these

additives and epsomite crystal surfaces is not a prerequisite for them to act as inhibitors. Overall, these additives are potentially applicable as growth inhibitors, retarders, or modifiers of epsomite growth, and, therefore, their industrial applications in processes requiring the control of scales or crystal shape could be of considerable relevance.

Finally, the combined use of in situ XRTD, in situ hot-stage ESEM, and kinetic thermal analyses is suggested as a novel approach to study thermally stimulated reactions. Such an approach may help in understanding the complex physical chemistry of organic−inorganic interactions that are relevant in many research fields: e.g., biomineralization and crystallization.

**Acknowledgment.** This work has been financially supported by the European Commission VIth Framework Program, under Contract No. SSP1-CT-2003-501571. Financial support has also been provided by the research group NRM-179 (Junta de Andalucía, Spain). The ESEM used is from CEAMA (Junta de Andalucía, Universidad de Granada). We thank M. A. Salas-Peregrín (Centro de Instrumentación Científica of the Universidad de Granada) for his help during TG and DSC analyses, I. Sanchez-Almazo (CEAMA) for her assistance during the ESEM study, and M. Bettini for editing of the original English manuscript. Comments and suggestions by Prof. Vyazovkin and two anonymous reveiwers are gratefully acknowledged.

## References and Notes

(1) Pina, C. M.; Putnis, C. V.; Becker, U.; Biswas, S.; Carroll, E. C.; Bosbach, D.; Putnis, A. *Surf. Sci.* **2004**, *553*, 61−74.
(2) House, W. A. *J. Colloid Interface Sci.* **1987**, *119*, 505−511.
(3) Amjad, Z. *Langmuir* **1991**, *7*, 600−603.
(4) Butt, F. H.; Rahman, F.; Baduruthamal, U. *Desalination* **1995**, *103*, 189−198.
(5) Ralston, P. H. *Mater. Protect. Perform.* **1972**, *11*, 39−44.
(6) van Rosmalen, G. M. *Chem. Eng. Commun.* **1983**, *20*, 209−233.
(7) Gu, P.; Ramachandran, V. S.; Beaudoin, J. J.; Quinn, E., *Adv. Cem. Based Mater.* **1995**, *2*, 182−188.
(8) Klepetsanis, P. G.; Koutsoukos, P. G. *J. Cryst. Growth* **1998**, *193*, 156−153.
(9) He, S.; Kan, A. T. a. T. M. B. *Appl. Geochem.* **1999**, *14*, 17−25.
(10) Tadros, M. E.; Mayes, I. *J. Colloid Interface Sci.* **1979**, *72*, 245−254.
(11) Amjad, Z. *Langmuir* **1993**, *9*, 597−600.
(12) Bosbach, D.; Hochella, M. F., Jr. *Chem. Geol.* **1996**, *132*, 227−236.
(13) Badens, E.; Veesler, S.; Boistelle, R. *J. Cryst. Growth* **1999**, *198/199*, 704−709.
(14) Oza, D. H.; Sapre, R. K. *Indian J. Technol.* **1976**, *14*, 435−437.
(15) Oner, M.; Dogan, O.; Oner, G. *J. Cryst. Growth* **1998**, *186*, 427−437.
(16) Rodríguez-Navarro, C.; Fernández, L.; Doehne, E.; Sebastian, E. *J. Cryst. Growth* **2002**, *243*, 503−516.
(17) Selwitz, C.; Doehne, E. *J. Cultural Heritage* **2002**, *3*, 20516.
(18) Chakraborty, D.; Agarwal, V. K.; Bhatia, S. K.; Bellare, J. *Ind. Eng. Chem. Res.* **1994**, *33*, 2187−2197.
(19) Cano, H.; Gabas, N.; Canselier, J. P. *J. Cryst. Growth* **2001**, *224*, 335−341.
(20) Wendlandt, W. W. *Thermal Method of Analysis*; John Wiley & Sons: New York, 1964.
(21) Rodante, F.; Catalani, G.; Vecchio, S. *J. Therm. Anal. Calorim.* **2002**, *68*, 689−713.
(22) Guarini, G. G. T.; Piccini, R. *J. Chem. Soc., Faraday Trans. 1* **1988**, *84*, 331−342.
(23) Ruiz-Agudo, E.; Rodriguez-Navarro, C.; Sebastián-Pardo, E. *Cryst. Growth Des.* **2006**, *6*, 1575−1583.
(24) Blitz, M.; Blitz, S.; Hughes, R.; Diner, B.; Beasley, R.; Knopp, J.; Rowe, B. H. *Chest* **2005**, *128*, 337−344.
(25) Fortes, A. D. *Axis* **2005**, *1*, 1−28.
(26) Ramalingom, S.; Podder, J.; Kalkura, S. N. *Cryst. Res. Technol.* **2001**, *36*, 1357−1364.
(27) Vaniman, D. T.; Bish, D. L.; Chipera, S. J.; Fialips, C. I.; William, Carey, J.; Feldman, W. C. *Nature* **2004**, *431*, 663−665.
(28) Ninan, K. N.; Nair, C. G. R. *Thermochim. Acta* **1979**, *30*, 25−35.
(29) Diefallah, E. H. M. *Thermochim. Acta* **1992**, *202*, 1−16.
(30) Stoilova, D.; Koleva, V. *Thermochim. Acta* **1996**, *290*, 85−91.
(31) Galwey, A. K. *Thermochim. Acta* **2000**, *355*, 181−238.
(32) Koga, N.; Tanaka, H. *Termochim. Acta* **2002**, *338*, 41−61.
(33) Heide, K. *J. Therm. Anal.* **1969**, *1*, 183−194.
(34) Hamad, S. el D. *Thermochim. Acta* **1975**, *13*, 409−418.
(35) Phadnis, A. B.; Deshpande, V. V. *Thermochim. Acta* **1981**, *43*, 249−250.
(36) Paulik, J.; Paulik, F.; Arnold, M. *Thermochim. Acta* **1981**, *50*, 105−210.
(37) Emons, H. H.; Ziegenbalg, G.; Naumann, R.; Paulik. F. *J. Therm. Anal. Calorim.* **1990**, *36*, 1265−1279.
(38) Ramalingom, S.; Podder, J.; Narayana Kalkura, S.; Bocelli, G. *J. Cryst. Growth* **2003**, *247*, 523−529.
(39) Popescu, C.; Jinau, V.; Alexandrescu, R.; Mihailescu, I. N.; Morjan, I.; Pascu, M. L. *Thermochim. Acta* **1988**, *129*, 269−276.
(40) Chou I. M.; Seal, R. R., II. *Astrobiology* **2003**, *3*, 619−630.
(41) Montgomery, D. R.; Gillespie, A. *Geology* **2005**, *33*, 625−628.
(42) McCord, T. B.; Orlando, T. M.; Teeter, G.; Hansen, G. B.; Sieger, M. T.; Petrik, N. G.; Van Keulen, L. *J. Geophys. Res., [Planets]* **2001**, *106*, 3311−3319.
(43) Garcia-Guinea, J.; Abella, R.; Snchez-Moral, S.; Benito, R.; Martin-Ramos, D. *J. Sediment. Res.* **2000**, *70*, 964−967.
(44) Correcher, V.; Garcia-Guinea, J.; Valle-Fuentes, F. J. *J. Therm. Anal. Calorim.* **2006**, *83*, 439−444.
(45) Rodriguez-Navarro, C.; Doehne, E. *Am. Lab.* **1999**, *31*, 28−35.
(46) Kloprogge, J. T.; Boström, T. E.; Weier, M. L. *Am. Mineral.* **2004**, *89*, 245−248.
(47) Romero Salvador, E.; García Calvo, C. *Termochim. Acta* **1992**, *203*, 67−76.
(48) Vecchio, S.; Materazzi, S.; Kurdziel, K. *Int. J. Chem. Kinet.* **2005**, *37*, 667−674.
(49) Vyazovkin, S. *Int. Rev. Phys. Chem.* **2000**, *19*, 45−60.
(50) Nishida, H.; Yamashita, M.; Hattori, N.; Endo, T.; Tokiwa, Y. *Polym. Degrad. Stab.* **2000**, *70*, 485−496.
(51) Vyazovkin, S.; Wight, C. A. *Thermochim. Acta* **1999**, *340−341*, 53−68.
(52) Burnham, A. K. *Thermochim. Acta* **2000**, *355*, 165−170.
(53) Vyazovkin, S. V. Lesnikovich, A. I. *Thermochim. Acta* **1999**, *340−341*, 53−68.
(54) Vyazovkin, S. V.; Dollimore, D. *J. Chem. Inf. Comput. Sci.* **1996**, *36*, 42−45.
(55) Vyazovkin, S. V.; Lesnikovich, A. I. *Thermochim. Acta* **1988**, *128*, 297−300.
(56) Mu, J.; Perlmutter, D. D. *Ind. Eng. Chem. Process Des. Dev.* **1981**, *20*, 640−646.
(57) McNeill, I. C.; Alston, A. *Angew. Makromol. Chem.* **1998**, *261/262*, 157−172.
(58) Ruiz-Agudo, E.; Rodriguez-Navarro, C.; Sebastian-Pardo, E. In *Heritage, Weathering and Conservation*; Fort, R., Alvárez de Buergo, M., Gómez-Heras, M., Vázquez-Calvo, C., Eds.; Balkema: Rotterdam, The Netherlands, 2006; pp 293−298.
(59) Coates, J. In *Encyclopedia of Analytical Chemistry*; Meyers R. A., Ed.; John Wiley & Sons: Chichester, U.K., 2000; pp 10815−10837.
(60) Dirksen, J. A.; Ring, T. A.; Duvall, K. N.; Jongen, N. *Int. J. Refrig.* **2001**, *24*, 856−859.
(61) Vyazovkin, S. V.; Lesnikovich, A. I. *Thermochim. Acta* **1990**, *165*, 273−280.
(62) Koga, N.; Tanaka, H. *J. Phys. Chem.* **1994**, *98*, 10521−10528.
(63) Tanaka, H.; Koga, N. *J. Phys. Chem.* **1988**, *92*, 7023−7029.